A Run-Group Proposal Submitted to PAC 44

Measurement of Deep Exclusive π^- Production using a Transversely Polarized ^{3}He Target and the SoLID Spectrometer

DRAFT: April 20, 2016

J. Arrington, K. Hafidi, P. Reimer, Z. Ye*

Argonne National Laboratory, Physics Division, Argonne, IL

H. Gao, X. Li, T. Liu, C. Peng, W. Xiong, X.F. Yan, Z. Zhao

Duke University, Durham, NC 27708, USA

E. Voutier

Institut de Physique Nucléaire IN2P3/CNRS, Université Paris Sud, 91406 Orsay, France

A. Camsonne, J-P. Chen

Jefferson Lab, Newport News, VA 23606, USA

M. Boer

Los Alamos National Laboratory, Physics Division, Los Alamos, NM

C. E. Hyde *Old Dominion University, Norfolk, VA*

Z. Ahmed*, G. Huber†

University of Regina, Regina, SK S4S 0A2, Canada

† Contact person

* Spokesperson

Contents

Abstract

We propose to measure the transverse nucleon, single-spin asymmetry $A_{UT}^{sin(\phi-\phi_s)}$ in the exclusive $\vec{n}(e,e'\pi^-)p$ reaction, during the transversely polarized ^{3}He target SIDIS experiment with SoLID. This polarization observable has been noted as being sensitive to the spin-flip generalized parton distribution (GPD) $\tilde{E}$, and factorization studies have indicated that precocious scaling is likely to set in at moderate $Q^2 \sim 2-4$ GeV^2, as opposed to the absolute cross section, where scaling is not expected until $Q^2 > 10$ GeV^2. Furthermore, this observable has been noted as being important for the reliable extraction of the charged pion form factor from pion electroproduction. The asymmetry data are projected to be of much higher quality than a pioneering measurement by HERMES [1].

This measurement is complementary to a proposal reviewed by PAC39 [2] for the SHMS+HMS in Hall C. The asymmetry that is most sensitive to $\tilde{E}$ is the longitudinal photon, transverse nucleon, single-spin asymmetry $A_L^{\perp}$ in exclusive charged pion electroproduction. The SHMS+HMS allow the L–T separation needed to reliably measure this quantity. However, the limited detector acceptance and the error-magnification inherent in an L–T separation necessitates the use of a next generation, externally polarized, continuous flow, high luminosity ^{3}He target based on a large volume polarizer and compressor being developed at the University of New Hampshire.

A wide $-t$ coverage is needed to obtain a good understanding of the asymmetry. Thus, it has always been intended to complement the SHMS+HMS $A_L^{\perp}$ measurement with an unseparated $A_{UT}^{sin(\phi-\phi_s)}$ measurement using a large solid angle detector. The high luminosity capabilities of SoLID make it well-suited for this measurement. Since an L–T separation is not possible with SoLID, the observed asymmetry is expected to be diluted by the ratio of the longitudinal cross section to the unseparated cross section. This was also true for the pioneering HERMES measurements, which provided a valuable constraint to models for the $\tilde{E}$ GPD.

1 Scientific Justification

1.1 Generalized Parton Distributions and Contribution from the Pion Pole

In recent years, much progress has been made in the theory of generalized parton distributions (GPDs). Unifying the concepts of parton distributions and of hadronic form factors, they contain a wealth of information about how quarks and gluons make up hadrons. The key difference between the usual parton distributions and their generalized counterparts can be seen by representing them in terms of the quark and gluon wavefunctions of the hadron. While the usual parton distributions are obtained from the squared hadron wavefunction representing the probability to find a parton with specified polarization and longitudinal momentum fraction x in the fast moving hadron (Fig. 1a), GPDs represent the interference of different wavefunctions, one where the parton has momentum fraction $x+\xi$ and one where this fraction is $x-\xi$ (Fig. 1b). GPDs thus correlate different parton configurations in the hadron at the quantum mechanical level. A special kinematic regime is probed in deep exclusive meson production, where the initial hadron emits a quark-antiquark or gluon pair (Fig. 1c). This has no counterpart in the usual parton distributions and carries information about $q\bar{q}$ and gg-components in the hadron wavefunction.

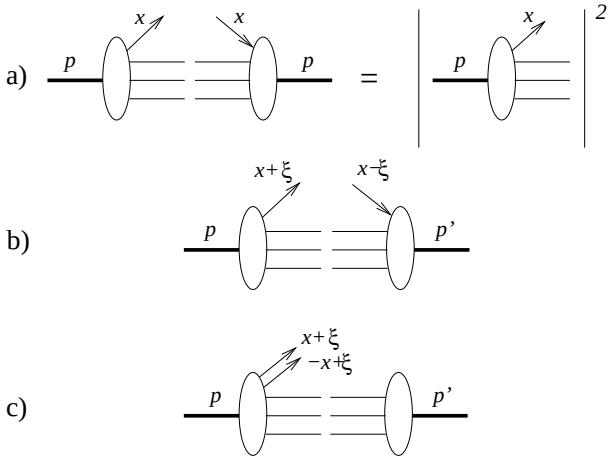

Figure 1: (a) Usual parton distribution, representing the probability to find a parton with momentum fraction x in the nucleon. (b) GPD in the region where it represents the emission of a parton with momentum fraction $x+\xi$ and its reabsorption with momentum fraction $x-\xi$. (c) GPD in the region where it represents the emission of a quark-antiquark pair, and has no counterpart in the usual parton distributions. This figure has been adapted from Ref. [3].

Apart from the momentum fraction variables x and ξ, GPDs depend on the four momentum transfer t. This is an independent variable, because the momenta p and p' may differ in either their longitudinal or transverse components. GPDs thus interrelate the longitudinal and transverse momentum structure of partons within a fast moving hadron.

In order to access the physics contained within GPDs, one is restricted to the hard scattering regime. An important feature of hard scattering reactions is the possibility to separate clearly the perturbative and nonperturbative stages of the interaction. Qualitatively speaking, the presence of a hard probe allows one to create small size quark-antiquark and gluon configurations, whose interactions are described by perturbative

QCD (pQCD). The non-perturbative stage of the reaction describes how the hadron reacts to this configuration, or how this probe is transformed into hadrons. This separation is the so-called factorization property of hard reactions. Deep Exclusive Meson electro-Production (DEMP) was first shown to be factorizable in Ref. [4]. This factorization applies when the virtual photon is longitudinally polarized, which is more probable to produce a small size configuration compared to a transversely polarized photon.

GPDs are universal quantities and reflect the structure of the nucleon independently of the reaction which probes the nucleon. At leading twist-2 level, the nucleon structure information can be parameterized in terms of four quark chirality conserving GPDs, denoted H, E, $\tilde{H}$ and $\tilde{E}$. H and E are summed over quark helicity, while $\tilde{H}$ and $\tilde{E}$ involve the difference between left and right handed quarks. H and $\tilde{H}$ conserve the helicity of the proton, while E and $\tilde{E}$ allow for the possibility that the proton helicity is flipped. Because quark helicity is conserved in the hard scattering regime, the produced meson acts as a helicity filter. In particular, leading order QCD predicts that vector meson production is sensitive only to the unpolarized GPDs, H and E, whereas pseudoscalar meson production is sensitive only to the polarized GPDs, $\tilde{H}$ and $\tilde{E}$. In contrast, deeply virtual Compton scattering (DVCS) depends at the same time on both the polarized ($\tilde{H}$ and $\tilde{E}$) and the unpolarized (H and E) GPDs. This makes DEMP reactions complementary to the DVCS process, as it provides an additional tool to disentangle the different GPDs [5].

Besides coinciding with the parton distributions at vanishing momentum transfer ξ, the GPDs have interesting links with other nucleon structure quantities. Their first moments are related to the elastic form factors of the nucleon through model-independent sum rules [6]:

$$\sum_q e_q \int_{-1}^{+1} dx H^q(x,\xi,t) = F_1(t), \tag{1}$$

$$\sum_q e_q \int_{-1}^{+1} dx E^q(x,\xi,t) = F_2(t), \tag{2}$$

$$\sum_q e_q \int_{-1}^{+1} dx \tilde{H}^q(x,\xi,t) = G_A(t), \tag{3}$$

$$\sum_q e_q \int_{-1}^{+1} dx \tilde{E}^q(x,\xi,t) = G_P(t), \tag{4}$$

where e_q is the charge of the relevant quark, $F_1(t)$, $F_2(t)$ are the Dirac and Pauli elastic nucleon form factors, and $G_A(t)$, $G_P(t)$ are the isovector axial and pseudoscalar nucleon form factors. The t-dependence of $G_A(t)$ is poorly known, and although $G_P(t)$ is an important quantity, it remains highly uncertain because it is negligible at the momentum transfer of β-decay [7]. Because of partial conservation of the axial current (PCAC), $G_P(t)$ alone receives contributions from $J^{PG} = 0^{--}$ states [8], which are the quantum numbers of the pion, and so $\tilde{E}$ contains an important pion pole contribution (Fig. 2a).

Accordingly, Refs. [9, 10] have adopted the pion pole-dominated ansatz

$$\tilde{E}^{ud}(x,\xi,t) = F_\pi(t) \frac{\theta(\xi > |x|)}{2\xi} \phi_\pi(\frac{x+\xi}{2\xi}), \tag{5}$$

where $F_\pi(t)$ is the pion electromagnetic form factor, and ϕ_π is the pion distribution amplitude.

$\tilde{E}$ cannot be related to already known parton distributions, and so experimental information about $\tilde{E}$ via DEMP can provide new information on nucleon structure which is unlikely to be available from any other source.

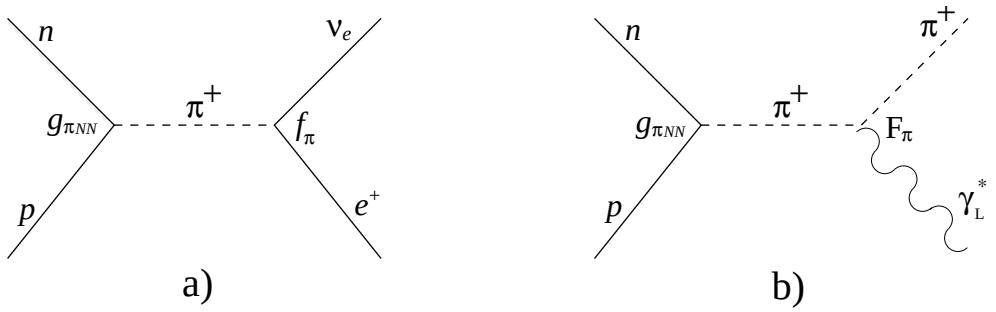

Figure 2: (a) Pion pole contribution to $G_P(t)$, and hence to $\tilde{E}$. (b) Pion pole contribution to meson electroproduction at low $-t$.

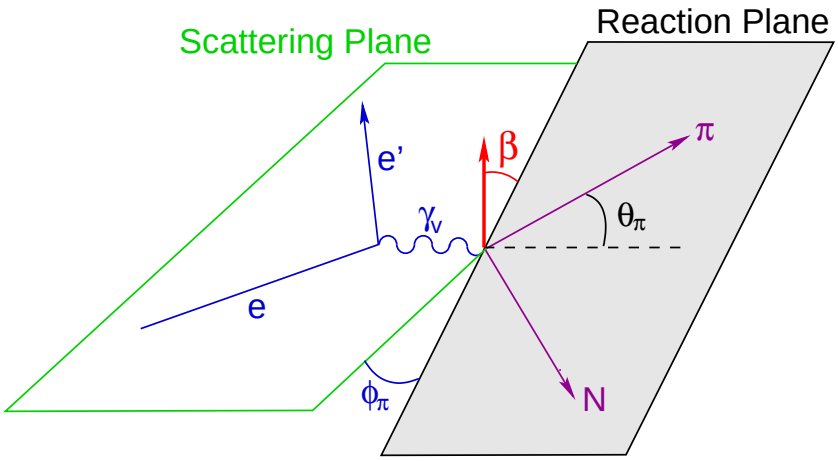

Figure 3: Scattering and hadronic reaction planes for exclusive $\vec{N}(e,e'\pi)N'$. β is the angle between the target nucleon polarization vector and the reaction plane. Some works alternatively label this angle as $(\phi - \phi_s)$.

1.2 Single spin asymmetry in exclusive pion electroproduction

Frankfurt et al. [11] have considered a specific polarization observable which is the most sensitive observable to probe the spin-flip $\tilde{E}$. This variable is the single-spin asymmetry for exclusive charged pion production, $\vec{p}(e,e'\pi^+)n$ or $\vec{n}(e,e'\pi^-)p$, from a transversely polarized nucleon target, and is defined [10] as

$$A_L^{\perp} = (\int_0^{\pi} d\beta \frac{d\sigma_L^{\pi}}{d\beta} - \int_{\pi}^{2\pi} d\beta \frac{d\sigma_L^{\pi}}{d\beta})(\int_0^{2\pi} d\beta \frac{d\sigma_L^{\pi}}{d\beta})^{-1}, \quad (6)$$

where $d\sigma_L^{\pi}$ is the exclusive charged pion electroproduction cross section using longitudinally polarized photons and β is the angle between the nucleon polarization vector and the reaction plane (Fig. 3). Frankfurt et al. [11] have shown that this asymmetry must vanish if $\tilde{E}$ is zero. If $\tilde{E}$ is not zero, the asymmetry will display a $\sin\beta$ dependence. Their predicted asymmetry using the $\tilde{E}$ ansatz from Ref. [12] is shown in Fig. 4. This calculation is Q^2-independent, depending only on how well the soft contributions cancel in the asymmetry.

It seems likely that a precocious factorization of the meson production amplitude into three parts – the overlap integral between the photon and pion wave functions, the hard interaction, and the GPD – will lead

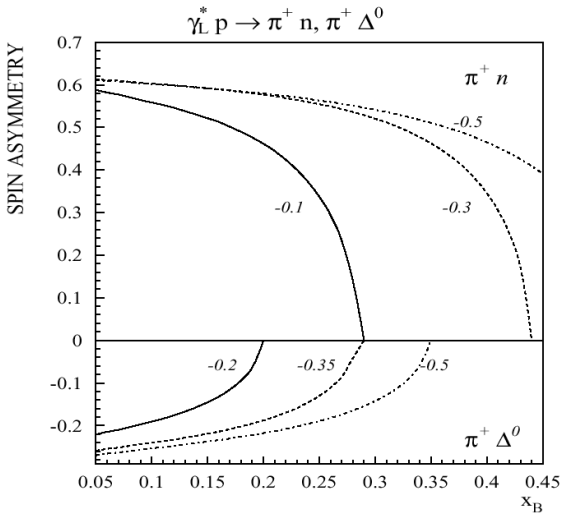

Figure 4: Transverse single-spin asymmetry for the longitudinal electroproduction of $\pi^+ n$ and $\pi^+\Delta^0$ at different values of t [indicated on the curves in GeV^2]. The asymmetry drops to zero at the parallel kinematic limit, which is different for each t value, because the definition of β is ill-defined at this point. This figure is taken from Ref. [13].

to a precocious scaling of $A_L^\perp$ as a function of Q^2 at moderate $Q^2 \sim 2-4$ GeV^2 [11]. This precocious scaling arises from the fact that higher order corrections, which are expected to be significant at low Q^2, will likely cancel when one examines the ratio of two longitudinal observables. In contrast, the onset of scaling for the absolute cross section is only expected for much larger values of $Q^2 > 10$ GeV^2.

This point is made clear in Fig. 5. This figure shows renormalon model calculations [14] of both the asymmetry and the longitudinal cross section at $Q^2 = 4$ GeV^2. While the magnitude of the cross section changes significantly when taking into account the twist-four corrections, $A_L^\perp$ is essentially insensitive to them and displays the expected precocious scaling. The relatively low value of Q^2 for the expected onset of precocious scaling is important, because it will be experimentally accessible after the Jefferson Lab 12 GeV upgrade. This places $A_L^\perp$ among the most important GPD measurements that can be made in the meson scalar. If precocious scaling cannot be experimentally demonstrated in this ratio of two cross sections, then it may not be possible to determine GPDs from DEMP data.

Refs. [5] and [13] also point out that the study of the transverse target single-spin asymmetry versus t is important for the reliable extraction of the pion form factor from electroproduction experiments (Fig. 2b). Investigations of hard exclusive π^+ electroproduction using a pQCD factorization model [15, 16] find that at $x_B = 0.3$ and $-t = -t_{min}$, the pion pole contributes about 80% of the longitudinal cross section. Since the longitudinal photon transverse single-spin asymmetry is an interference between pseudoscalar and pseudovector contributions, its measurement would help constrain the non-pole pseudovector contribution, and so assist the more reliable extraction of the pion form factor. The upper $Q^2 = 6$ GeV^2 limit of the approved pion form factor measurements in the JLab 12 GeV program [17] is dictated primarily by the requirement $-t_{min} < 0.2$ GeV^2, to keep non-pion pole contributions to σ_L at an acceptable level [16]. Transverse target single-spin asymmetry studies versus t may eventually allow, with theoretical input, the

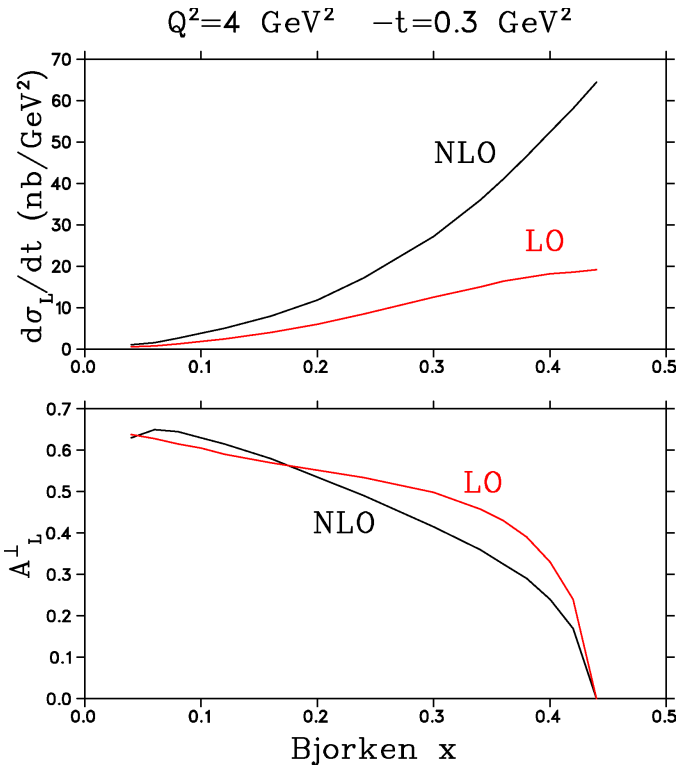

Figure 5: Calculation of the longitudinal photon transverse nucleon spin asymmetry including twist-four corrections by A. Belitsky [14] at $-t = 0.3$ GeV^2, Q^2=4 GeV^2. The red curves are the leading order calculation, while the black curves have twist-four power effects taken into account. While the cross section is very sensitive to these corrections, the transverse spin asymmetry is stable.

use of somewhat larger $-t$ data for pion form factor measurements, ultimately extending the Q^2-reach of pion form factor data acquired with JLab 12 GeV beam. Thus, measurements of the transverse single-spin asymmetry are a logical step in the support of the pion form factor program.

1.3 The Complementarity of Separated and Unseparated Asymmetry Measurements

The reaction of interest is $^3He(e,e'\pi^-)p(pp)_{sp}$. The measurement of the transverse single-spin asymmetry requires the detection of the π^- in non-parallel kinematics. It is the component of the target polarization parallel to $\hat{q} \times \hat{p_\pi}$ that is important, and this direction is uniquely defined only in non-parallel kinematics.

Experimentally, the angle between the target polarization and the reaction plane, β, and the angle between the scattering and reaction planes, ϕ, are not independent. If the target polarization is at some angle, ϕ_s, relative to the scattering plane, then $\beta = \phi_s - \phi$. The polarized nucleon cross section can be

expressed in terms of these variables as:

$$\begin{aligned}\sigma_t = &-P_\perp \sin\beta\,[\sigma_{TT}^y + 2\epsilon\,\sigma_L^y] \\ &- P_\perp \sin\beta\,[\epsilon(\cos 2\phi_s \cos 2\beta + \sin 2\phi_s \sin 2\beta)\,\sigma_{TT'}^y] \\ &- P_\perp \sin\beta\left[\sqrt{2\epsilon(1+\epsilon)}(\cos\phi_s\cos\beta + \sin\phi_s\sin\beta)\,\sigma_{LT}^y\right] \\ &- P_\perp \cos\beta\left[\sqrt{2\epsilon(1+\epsilon)}(\sin\phi_s\sin\beta - \cos\phi_s\cos\beta)\,\sigma_{LT}^x\right] \\ &- P_\perp \cos\beta\,[\epsilon(\sin 2\phi_s \sin 2\beta - \cos 2\phi_s \cos 2\beta)\,\sigma_{TT}^x]\,. \quad (7)\end{aligned}$$

From the above equation, it is clear that to extract $A_L^\perp$ it is necessary to first isolate the $\sin\beta$ Fourier component of the polarized nucleon cross section. Once that has been accomplished, one must then separate the σ_L^y term from the σ_{TT}^y term via a Rosenbluth-type separation.

It has not yet been possible to perform an experiment to measure $A_L^\perp$. The conflicting experimental requirements of transversely polarized target, high luminosity, L–T separation, and closely controlled systematic uncertainty, make this an exceptionally challenging observable to measure. The SHMS+HMS is the only facility with the necessary resolution and systematic error control to allow a measurement of $A_L^\perp$. However, the beamtime required to do a good measurement with current polarized target technology is in the range of 10^3 days. To minimize the beamtime required, PR12-12-005 proposed the use of a next generation, externally polarized, continuous flow, high luminosity ^{3}He target based on a large volume polarizer and compressor developed at the University of New Hampshire [2]. The science case for this measurement was favorably reviewed by PAC39, and they encouraged the continued development of the target technology. Although the New Hampshire group is making continued progress on the development of the target, there is no timeline for its actual implementation at Jefferson Lab.

The most closely related measurement, of the transverse single-spin asymmetry in exclusive π^+ electroproduction without an L–T separation, was published by the HERMES Collaboration in 2010 [1]. Their data were obtained for average values of $\langle x_B\rangle = 0.13$, $\langle Q^2\rangle = 2.38$ GeV^2 and $\langle t'\rangle = -0.46$ GeV^2, subject to the criterion $W^2 > 10$ GeV^2. The six Fourier amplitudes in terms of the azimuthal angles ϕ, ϕ_s of the pion-momentum and proton-polarization vectors relative to the lepton scattering plane were determined. Of these, at leading twist only the $\sin(\phi-\phi_s)_{UT}$ Fourier amplitude receives a contribution from longitudinal photons. If one assumes that longitudinal contributions dominate, these $A_{UT}^{sin(\phi-\phi_s)}$ values can be compared to GPD models for $\tilde{E}$, $\tilde{H}$.

Because transverse photon amplitudes are suppressed by $1/Q$, at very high Q^2 it is safe to assume that all observed meson production is due to longitudinal photons. At the lower Q^2 typical of the JLab and HERMES programs, however, this is not the case. Calculations by Goloskokov and Kroll [18] indicate much of the unseparated cross section measured by HERMES [1] is due to contributions from transversely polarized photons. In addition, there are contributions to $A_{UT}^{sin(\phi-\phi_s)}$ from the interference between two amplitudes, both for longitudinal photons, as well as transverse photons [19]. As indicated in Fig. 6, the contribution from transverse photons tends to make the asymmetry smaller. At the HERMES kinematics, the dilution caused by transverse photons is about 50%.

A run-group proposal concurrent with the SoLID transversely polarized ^{3}He SIDIS experiment allows for an unseparated asymmetry measurement to be obtained on a sooner timescale than the Hall C measurement. In comparison to the HERMES measurement, the experiment proposed here will probe higher Q^2 and x_B,

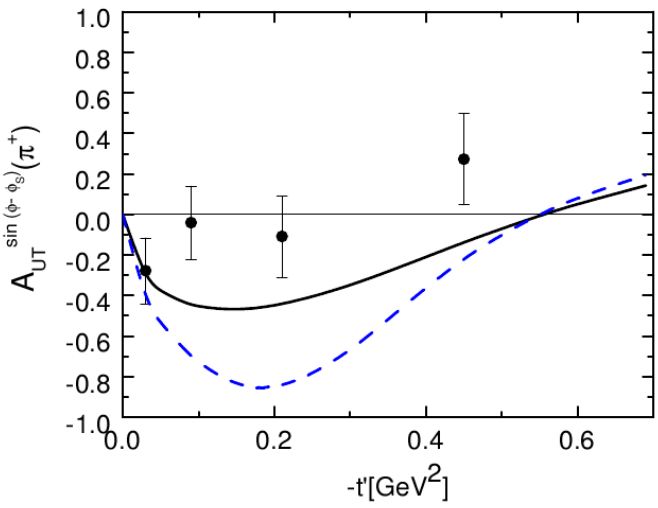

Figure 6: Predictions by Goloskokov and Kroll for the $\sin(\phi-\phi_s)$ moment of A_{UT} in the handbag approach, in comparison to the data from HERMES at $Q^2 = 2.45$ GeV^2, $W = 3.99$ GeV. The independent variable is $-t' = |t - t_{min}|$. Dashed line: contribution from longitudinal photons only. Solid line: full calculation including both transverse and longitudinal photons. This figure is taken from Ref. [18].

with much smaller statistical errors over a wider range of $-t$. SoLID will allow the first measurement for $Q^2 > 4$ GeV^2, where GPD-based calculations are expected to apply. Thus, the measurements should be more readily interpretable than those from HERMES. Similar measurements using CLAS-12 and a transversely polarized ^{1}H target have been discussed previously [22], but this measurement will allow for smaller statistical uncertainties, due to SoLID's higher luminosity capabilities.

Handbag model calculations by Goloskokov and Kroll [20] shed further light on the expected asymmetry dilution. The lower left panel of Fig. 7 shows their predictions for the cross section components in exclusive charged pion production. Although their calculations tend to underestimate the σ_L values measured in the JLab $F_\pi - 2$ experiment [21], their model is in reasonable agreement with the unseparated cross sections [18]. They predict significant transverse contributions for JLab kinematics. A comparison of the unseparated asymmetry at $-t = 0.3$ GeV^2, $x_B = 0.365$ in Fig. 7 with the separated longitudinal asymmetry at the same values of x_B, $-t$ in Fig. 5 indicates a substantial dilution of the unseparated asymmetry due to transverse photon contributions, similar to that observed in Fig. 6.

In addition to allowing a measurement at $Q^2 > 4$ GeV^2, a measurement by SoLID of $A_{UT}^{sin(\phi-\phi_s)}$ will cover a fairly large range of $-t$, allowing the asymmetry to be mapped over its full range with good statistical uncertainties – from its required zero-value in parallel kinematics, through its maximum, and then back to near-zero as σ_T dominates σ_L at larger $-t$. The shape of the asymmetry curve versus $-t$, as well as its maximum value, are critical information for comparison to GPD-based models. At a later date, the New Hampshire polarized target might enable a measurement of $A_L^\perp$ in Hall C. Although undiluted, the error-magnification inherent in an L–T separation will make for larger uncertainties. The comparison of the maxima and t-dependences of both measurements will provide complementary data needed to extract $\tilde{E}$ information and better understand non-pole contributions complicating the extraction of the pion form

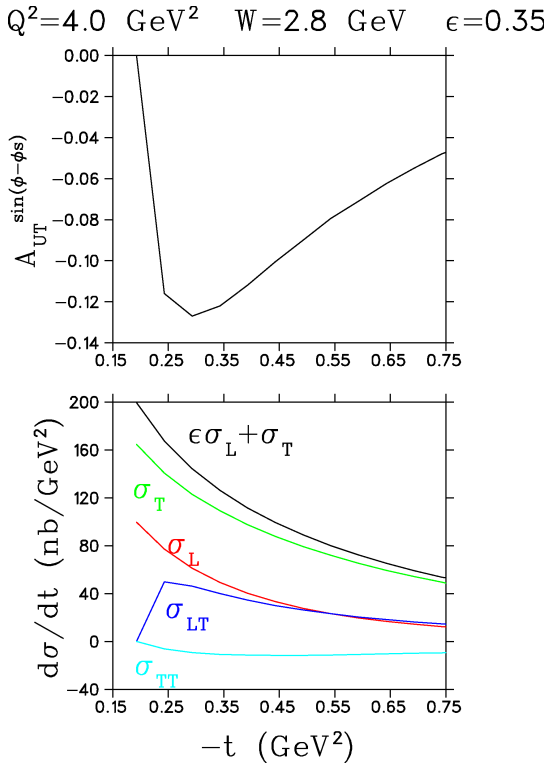

Figure 7: Calculation of the cross section components and $\sin(\phi - \phi_s)$ moment of the transverse nucleon spin asymmetry A_{UT} in the handbag approach by Goloskokov and Kroll [20] for kinematics similar to those in Fig. 5. Our measurement will be at higher $0.55 < \epsilon < 0.75$ than the $\epsilon = 0.35$ kinematics of this figure, so the dilution in the asymmetry will be significantly less.

factor from electroproduction data.

2 Experimental Method

We propose to carry out the $^3He(e,e'\pi^-)p(pp)_{sp}$ measurement using the Solenoidal Large Intensity Device (SoLID [25]), in parallel with the already approved experiment, E12-10-006 [24], which will measure Semi-Inclusive Deep-Inelastic Scattering (SIDIS). There are two SoLID configurations, called SoLID-SIDIS and SoLID-PVDIS. Besides E12-10-006, two SIDIS experiments, E12-11-007 [26] and E12-11-108 [27], along with the J/ψ experiment (E12-12-006 [28]), will use the SoLID-SIDIS configuration. All of these experiments have been approved with A or A- rating. In addition, two "bonus-run" experiments, E12-10-006A [30] and E12-11-108A [**?**], have also been approved to run in parallel with the SIDIS experiments. The SoLID-PVDIS configuration is for the Parity Violation in Deep Inelastic Scattering (PVDIS).

The experiment will use a near identical setup as E12-10-006, but with few additions without affecting the approved experiment. We will use exactly the same online production trigger, which is the coincidence of electron triggers and hadron triggers. However, we request to add a new trigger type on top of the existing ones to identify the proton events for the offline triple coincidence analysis. The SoLID-SIDIS detector can only detect protons with scattering angles from 8° up to 24°, while the main proton events from the DEMP process can cover up to 65°. We propose to add a new proton detector based on scintillator counters to detect protons from 24° to 65°. The new detector will be placed between the target system and the entrance and of CLEO-II magnet. The new proton trigger and the new proton detector will be discussed in more detailed in the following sections.

2.1 Transversely Polarized ^{3}He Target

The proposed measurement will utilize the same polarized ^{3}He target as E12-10-006 [**?**]. Such a target was successfully employed in E06-110, a 6 GeV SIDIS experiment in Hall A. A wide range of experiments have utilized polarized ^{3}He as an effective neutron target over a wide range of kinematics. And over the past decades several authors have calculated the effective neutron polarizations in ^{3}He using three-nucleon wave functions and various models of the $N-N$ interaction [23]. These are now well established, and the error introduced by uncertainty in the wave functions are small.

Other nuclear effects which can influence the experimental asymmetry for a neutron bound inside ^{3}He include, Fermi motion, off-shell effects, meson exchange currents, delta isobar contributions and π^- final state interactions. The exclusive nature of the process, the selected kinematics such as high Q^2, large recoil momentum and a complete coverage of the azimuthal angle ϕ ensures that corrections due to these nuclear effects will be small and can be modeled effectively.

Target	^{3}He
Length	40 cm
Target Polarization	∼60%
Target Spin Flip	≤20 mins
Target Dilution	90%
Effective Neutron	86.5%
Target Polarimetry Accuracy	∼ 3%

Table 1: Key Parameters of the ^{3}He target.

The ^{3}He polarization direction is held by three sets of Helmholtz coils with a 25 Gauss magnetic field. Both the transverse and longitudinal directions can be provided by rotating the magnetic field. The ^{3}He gas with density of about 10 atm (at 0°) is stored in a 40 cm target cell made of thin glasses. With a 15 μA electron beam, the neutron luminosity can be as high as $10^{36} cm^{-2} s^{-1}$. In-beam polarization of 60% was archived during the E06-110 experiment. Two kinds of polarimetry, NMR and EPR, were used to measure the polarization with relative 5% precision. We have planed to improve the accuracy of the measurement to reach 3%.

The target spin will be reversed for every 20 minutes by using the RF AFP technique. The additional polarization loss due to the spin reversal was kept at < 10 % which has been taken into account in the overall 60% in-beam polarization. A new method for spin reversal using field rotation has been tested and was able to eliminate the polarization loss. Such an improvement will enable us to perform the spin-reversal in few minutes to reduce the target-spin-correlated systematic errors. The key parameters of the ^{3}He target are summarized in Table 1.

A collimator, similar to the one used in the E06-110, will be placed next to the target cell window to minimize the target cell contamination and to reduce the event rate. Several calibration targets will also be installed in this target system, including a multi-foil ^{12}C for optics study, a BeO target for beam tuning, and a reference target cell for dilution study and other calibration purposes.

2.2 SoLID Spectrometer and Detectors

The solenoid magnet for SoLID will be based on the CLEO-II magnet built by Cornell University. The magnet is 3 meters long with the out diameter of 3 meters and the inner diameter of 1 meter. The field strength is greater than 1.35 Tesla with integrated BDL of 5 Tesla-meters. The fringe field at the front end after shielding is less than 5 Gauss. In the SIDIS-configuration, the CLEO-II magnet provides 2π acceptance in the azimuthal angle (ϕ) and covers the polar angle (θ) from 8° up to 24°. The momentum acceptance is between 0.8 and 7.5 GeV/c and the momentum resolution is about 2%.

The layout of the SoLID detectors in the SIDIS-configuration is shown in Fig. 8. The detector system is divided into two regions for the forward-angle (FA) detection and the large-angle (LA) detection. Six Gas Electron Multiplier (GEM) tracking chambers will be used for charged particle tracking, where only the first four of them will be used for the large-angle detection. In each region, a Shashlyk-type sampling EM calorimeter (LAEC or FAEC) will measure the particle energy and identify electrons from hadrons. A scintillator-pad detector (LASPD and FASPD) will be installed in front of each EC to reject photons and provide timing information. The forward-angle detectors will detect both the electrons and hadrons (mainly $\pi^{\pm}$). A light-gas Čerenkov detector (LGC) and a heavy-gas Čerenkov detector (HGC) will perform the $e/\pi^{\pm}$ and $\pi^{\pm}/K^{\pm}$ separation, respectively. The Multi-gas Resistive Plate Chamber (MRPC) will provide a precise timing measurement and serve as a backup of the FASPD on photon rejection. A more detailed discussion of the design, simulation, prototype-test of each detector is given in the SoLID preliminary conceptual design report (pCDR) [25].

Table 2 summarizes the key parameters of the detector system in the SIDIS configuration for both the SIDIS and DEMP measurements.

Experiments	SIDIS	DEMP
Reaction channel	$\vec{n}(e,e'\pi^{\pm})X$	$\vec{n}(e,e'\pi^{-}p)$
Target	^{3}He	same
Unpolarized luminosity	$\sim 10^{37}$ cm^{-2}s^{-1} per nucleon	same
Momentum coverage	0.8-7.5 (GeV/c)	same
Momentum resolution	$\sim$2%	same
Azimuthal angle coverage	0° 360°	same
Azimuthal angle resolution	5 mr	same
Polar angle coverage	8°-24° for e	same
Polar angle coverage	8°-14.8° for $\pi^{\pm}$	same
		8°-24 ° for p
		24°-65° for p with recoil detector
Polar angle resolution	0.6 mr	same
Target Vertex resolution	0.5 cm	same
Energy resolution on ECs	5%$\sim$10%	same
Trigger type	Double Coincidence $e^- + \pi^{\pm}$	Triple Coincidence $e^- + \pi^- + p$
Expected DAQ rates	<100 kHz	same online (<30 Hz offline)
Main Backgrounds	(e,e'K$^{\pm}$) Accidental Coincidence	(e,e'$\pi^{\pm}$) Accidental Coincidence
Key requirements	Radiation hardness Kaon Rejection DAQ	Radiation hardness Proton Detection

Table 2: Summary of Key Parameters for DEMP Measurement compared with SIDIS Experiments.

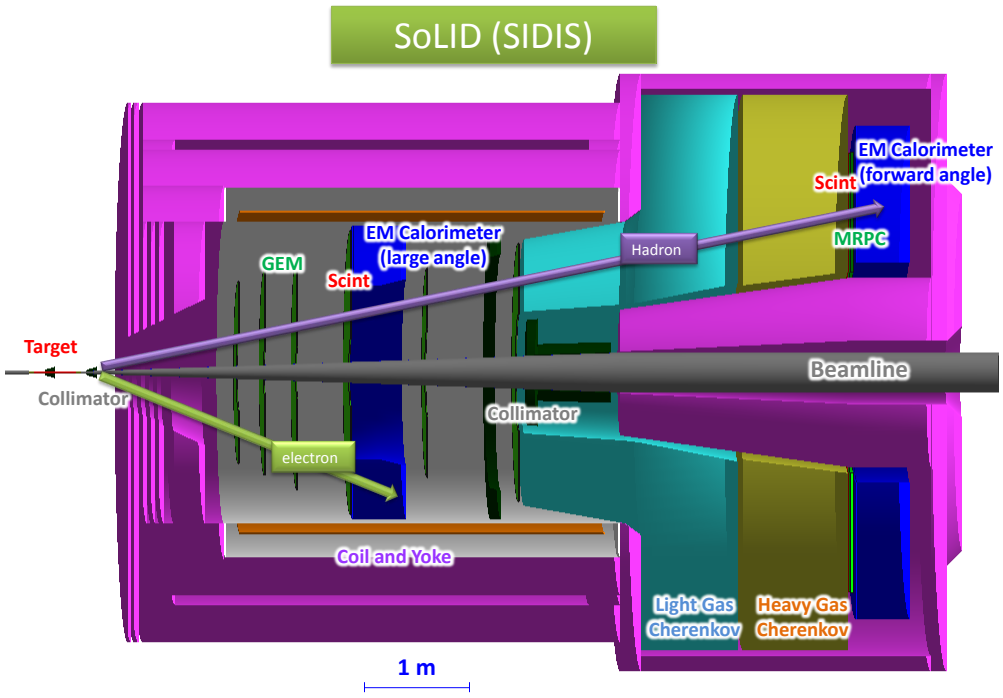

Figure 8: The Detector Layout of the SoLID-SIDIS configuration. The detector system includes six Gas Electron Multiplier (GEM) planes for charged particle tracking, two Scintillator Pad Detectors (SPD) followed by two Shashlyk sampling EM Calorimeters (EC) for energy measurement and particle identification, a Light Gas Čerenkov Detector (LGC) for e-$\pi^{\pm}$ separation, a Heavy Gas Čerenkov Detector (HGC) for $\pi^{\pm}$-$K^{\pm}$ separation, as well as a Multi-gap Resistive Plate Chamber (MRPC) for timing measurement. The first four GEM trackers, the first SPD (i.e. LASPD) and EC (i.e. LAEC) form the large-angle detection system for electron measurement. The forward-angle detection system, to measure electron and hadrons, is composed of all six GEM trackers, LGC, HGC, MRPC, the second SPD (i.e. FASPD) and the second EC (FAEC). The photon-detection in the large-angle is given by the veto-signal of the SPD in coincidence with the EC signal, where the photons in the forward-angle system will be triggered by the EC signal plus the veto-signals of LGC, SPD, and MRPC.

2.3 A Proton Recoil Detector

In the SoLID-SIDIS detector system, protons can be isolated from other hadronic events by using the time-of-fly (TOF) information which requires the timing to be as good as **100** ps (**Check it!**).

2.4 Trigger Design

In E12-10-006, the online production trigger will be the double-coincidence of the scattered electrons and hadrons. One will use the particle identification detectors, such as LGC, HGC and ECs, during the offline analysis to select $\pi^{\pm}$ out from other hadrons. The DEMP events will be identified with the triple-coincidence trigger of the scattered electron, π^{-} and proton. We will use the same online trigger as the SIDIS one, and hence the new experiment will share the same data set as E12-10-006. However, a new trigger type will be added to the DAQ system to record recoil proton events, and we will perform the offline analysis to isolate the triple-coincidence events..

The proton trigger will be produced in two regions, the new proton recoil detector and the standard

SoLID timing detectors (e.g., MRCP and LASPD).

The actual trigger design will be far more complicated, and the detailed discussion of the trigger and DAQ design has been given in the SoLID pCDR [25].

3 Projected Results

3.1 Kinematic Coverage

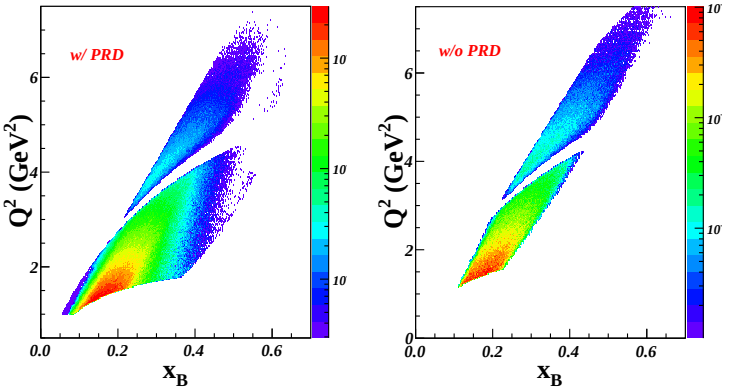

Figure 9: The kinematic coverage at different acceptances at 11 GeV. The left plot shows the coverage when detecting all recoil protons, while the right plot shows the coverage with proton detection by existing SoLID detectors. Colors correspond to rates (Hz) in log scale.

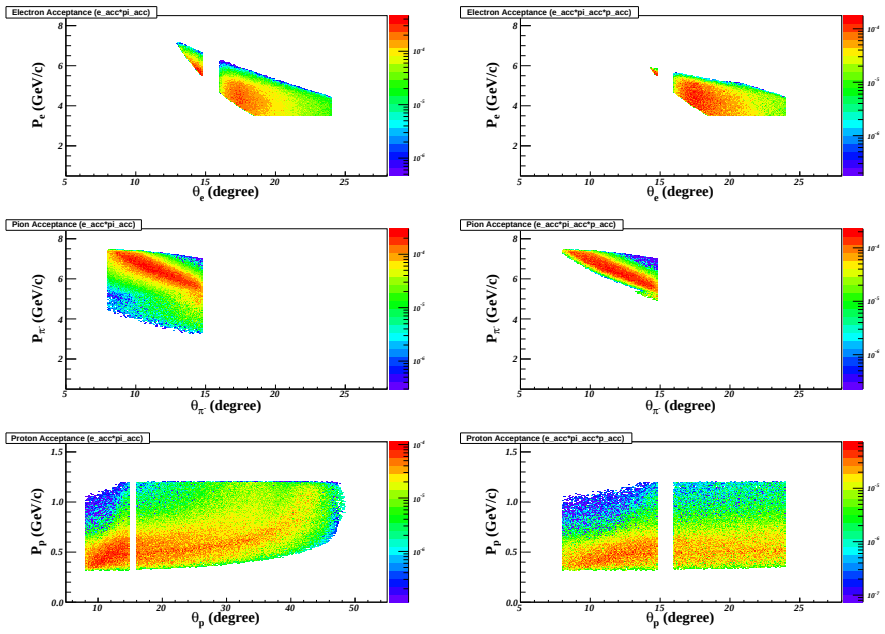

(a) w/ PRD (b) w/o PRD

Figure 10: The acceptance of the momenta and polar angles w/ or w/o the PRD. In each panel, the top, middle and bottom plots are for electrons, π^- and protons, respectively. A cut of $Q^2 > 4$ GeV^2 is applied. Colors correspond to rates (Hz) in log scale.

The kinematic coverage in $Q^2 vs. x_B$ is shown in Fig. 9 where two proton detection cases were given: (a) by

using existing SoLID detectors to detect protons at small angles ($8^\circ \sim 24^\circ$) and adding a new proton recoil detector to detect rest of recoil protons at large angle ($24^\circ \sim 65^\circ$), or (b) by only using the existing SoLID detectors. These distributions were weighted by the DEMP cross sections and the spectrometer acceptance obtained from the GEANT4 simulation with the SIDIS configuration. As shown in these plots, the range of Q^2 is from 1.0 GeV^2 to 8.0 GeV^2, x_B goes from 0.1 up to 0.75.

Fig. 10 shows the momentum and angular acceptance of electrons, π^- and protons which form the DEMP events and can be detected with the SoLID detectors and (or) with the new PRD. A cut of Q$^2 > 4$ GeV^2 is applied since most of valid DEMP events are at high Q^2. The recoil protons shown in Fig. 10 have low momenta ranged from 0.3 GeV/c up to 1.2 GeV/c and their rates distribute near uniformly along the scattering angle.

3.2 Estimated Rates

$1 <$ Q$^2 < 4$ GeV^2	Q$^2 > 4$ GeV^2	Total
DEMP: $\vec{n}(e, e'\pi^- p)$ Triple-Coincidence (Hz)		
17.79 (0.22)	0.53 (0.31)	26.45 (7.66)
SIDIS: $\vec{n}(e, e'\pi^-)X$ Double-Coincidence (Hz)		
1388.85	35.77	1424.62

Table 3: Triple-Coincidence rates for DEMP events compared with the SIDIS rates. Numbers in brackets are the DEMP rates with only detecting protons using existing SoLID detectors. The online production trigger will be the SIDIS double-coincidence trigger of which rates are also given.

Table 3 lists the triple-coincidence rate of the DEMP events. The rates were calculated with the simulated events weighted by the target luminosity, the SoLID acceptances and cross sections. The rates are the unpolarized event rates and are not corrected by the beam and target polarization, target dilution and so on. The total integrated physics rate is estimated to be around 26 Hz at 11 GeV, or 0.53 Hz at Q$^2 > 4$ GeV^2. If only using the existing SoLID detectors to detect protons, the rate drops to 0.31 Hz at Q$^2 > 4$ GeV^2. For comparing, the table also gives the SIDIS rate which will be the online production trigger rates and is the main background of the DEMP events.

3.3 Asymmetry Projections

The proposed new experiment will run in parallel with E12-10-006 of which total beam time of 48 days at E_0=11 GeV has been approved. As shown in Fig. 11, We defined 7 $-t$ bins of which the the boundaries are defined by the array:

$$-t[8] = [0.0, 0.15, 0.25, 0.35, 0.45, 0.55, 0.75, 1.10] \quad (in\ GeV^2) \tag{8}$$

The number of events (N_i) in the ith bin is calculated with the total simulated events after applying cuts on important kinematic variables, e.g. $Q^2 >$4 GeV$^2, W > 2\ GeV, 0.55 < \epsilon < 0.75$ and $t_{min} < t < t_{max}$. As shown in Eq. 9, each event survived the cuts then is weighted by the unpolarized cross section, the acceptance of the electron, pion and photon. N_i is further corrected by the phase-space (PSF) defined

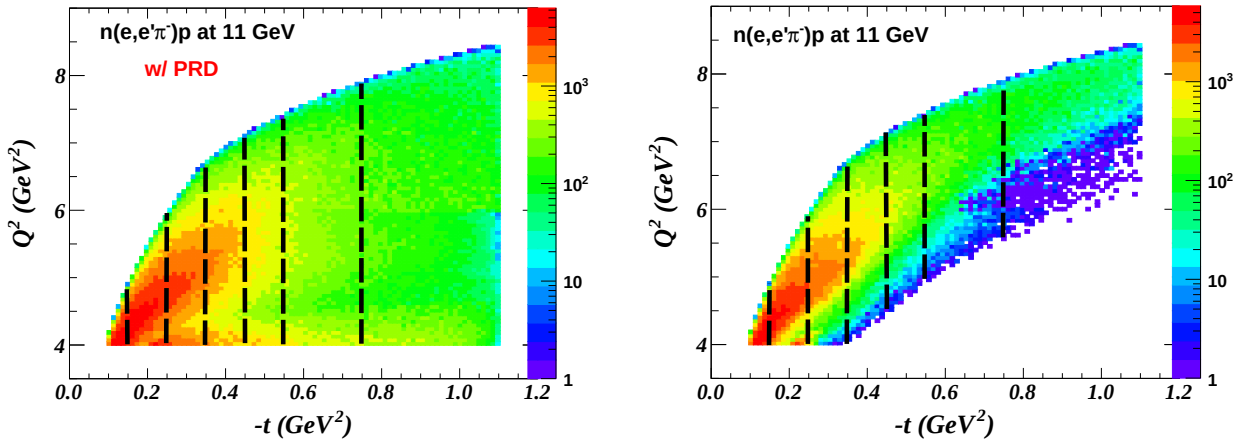

(a) w/ PRD

(b) w/o PRD

Figure 11: Q^2 vs. $-t$ where the black dash lines specify the boundaries of 7 $-t$ bins. The color panel indicates the raw counts with 48 days of beam time at 11!GeV and assuming protons to be detected only by existing SoLID detectors.

in the event generator to randomly generate a total number of events (N_{gen}), beam-time (T), the target luminosity ($L = 10^{36} cm^{-2} s^{-1}$), and the overall detector efficiency (ϵ_{eff}):

$$N_i = (\sum_{j \in i-bin} \sigma_j^{avg} \cdot A_j^e \cdot A_j^{\pi^-} \cdot A_j^p) \cdot (PSF/N_{gen}) \cdot T \cdot L \cdot \epsilon_{eff}, \tag{9}$$

where j is the jth event in the ith bin, σ_j^{avg} is the cross section of the event. $A_j^{e(\pi^-,p)}$ is the acceptance weight of the electron (pion, proton) in this event. The detector efficiency, ϵ_{eff}, is fixed at 85%. N_i corresponds to the raw experimental count of electrons scattering on neutrons in ^{3}He before taking into account the target polarization ($P \sim 60\%$), the effective polarization of neutrons ($\eta_n \sim 86.5\%$) and the dilution effect from other reaction channels when electrons scattering on ^{3}He ($f \sim 90\%$). The statistical error of the target single spin asymmetry (A_{UT}) in each bin can be given as:

$$\delta A_{UT} = \frac{1}{P \cdot \eta_n \cdot f} \sqrt{\frac{1 - (P \cdot < A_{UT} >)^2}{N_i^+ + N_i^-}}, \tag{10}$$

where $N_i^{+(-)}$ is the number of counts in each bin when the target polarization is up (down), and we easily have $N_i = N_i^+ + N_i^-$; $< A_{UT} >$ is the average asymmetry in the bin. As shown in Appendix. A, A_{UT} is predicted with a phenomenological model, but because of not performing a L/T separation in this experiment, the asymmetry should be corrected by another dilution factor which is defined as:

$$f_{L/T} = \frac{\epsilon \cdot \sigma_L}{\sigma_T + \epsilon \cdot \sigma_L}, \tag{11}$$

where $\epsilon = 1/(1 + \frac{2\nu}{Q^2} tan^2(\theta))$ and additional dilution due to σ_{TT} is assumed to be small. Hence, $A_{UT} = f_{L/T} \cdot A_{UT}^{model}$.

Fig. 12 shows the distribution of A_{UT} vs. $-t$ with projected statistical errors discussed above. Compared with the existing HERMES results (Fig. 6), the new measurement could provide more precious data to be directly compared with theoretical predictions. The detailed information of each bin has been listed in Table 4

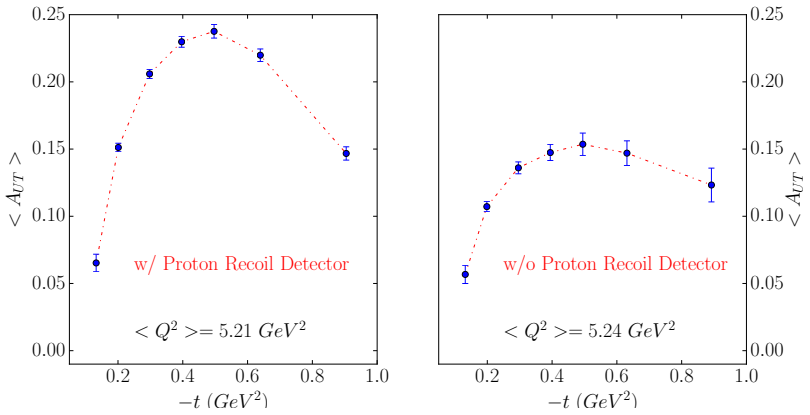

Figure 12: Projection of target sing spin asymmetry (A_{UT}) in $-t$ binning for DEMP with transversely polarized ^{3}He at E_0=11 GeV. The error bars are the projected statistical uncertainties defined in Eq. 10. The asymmetry value in each bin is predicted with the model given in Appendix. A and is diluted due to not separating the L/T contributions. The left plot shows the projection w/o a new proton recoil detector while the right plot shows a better ojected result with the new detector. One can see the average asymmetries are also changed between two configurations and it is because the asymmetry strongly depends on Q^2 which changes w/ or w/o the PRD.

w/ PRD	Bin#1	Bin#2	Bin#3	Bin#4	Bin#5	Bin#6	Bin#7
$< -t >$	0.13	0.20	0.30	0.40	0.50	0.64	0.90
$< Q^2 >$	4.22	4.59	5.02	5.38	5.64	5.90	6.27
$< A_{UT} >$	6.53×10^{-2}	1.51×10^{-1}	2.06×10^{-1}	2.30×10^{-1}	2.38×10^{-1}	2.20×10^{-1}	1.47×10^{-1}
δA_{UT}	6.50×10^{-3}	3.15×10^{-3}	3.36×10^{-3}	4.05×10^{-3}	5.02×10^{-3}	4.64×10^{-3}	4.95×10^{-3}
N	6.55×10^{4}	2.78×10^{5}	2.43×10^{5}	1.66×10^{5}	1.08×10^{5}	1.27×10^{5}	1.13×10^{5}

w/o PRD	Bin#1	Bin#2	Bin#3	Bin#4	Bin#5	Bin#6	Bin#7
$< -t >$	0.13	0.20	0.30	0.39	0.49	0.63	0.89
$< Q^2 >$	4.22	4.67	5.23	5.78	6.26	6.81	7.59
$< A_{UT} >$	5.67×10^{-2}	1.07×10^{-1}	1.36×10^{-1}	1.47×10^{-1}	1.54×10^{-1}	1.47×10^{-1}	1.23×10^{-1}
δA_{UT}	6.76×10^{-3}	3.73×10^{-3}	4.42×10^{-3}	5.92×10^{-3}	8.30×10^{-3}	9.15×10^{-3}	1.26×10^{-2}
N	6.07×10^{4}	1.99×10^{5}	1.41×10^{5}	7.87×10^{4}	4.00×10^{4}	3.29×10^{4}	1.75×10^{4}

Table 4: Detailed information of projected bins from the new DEMP measurements with SoLID, while $< Q^2 >$ and $< -t >$ are in the unit of GeV^2. The top (bottom) table is with respect to the case of proton detection w/ (w/o) a new PRD.

4 Missing Mass and Background

The dominated background of the DEMP measurements comes from the SIDIS reactions of electrons scattering on the neutron and two protons in ^{3}He. In addition to detect the recoil proton, we also rely on reconstructing the neutron missing mass spectrum to ensure the exclusivity of the DEMP events. In SIDIS, however, the final states include the scattered electron, the hadrons ($\pi^{\pm}$, $K^{\pm}$ etc.), as well as the undetected target fragments which could contain protons.

We studied the contamination of the SIDIS events in the DEMP missing mass spectrum. The SIDIS

reactions, $p(e,e'\pi^-)X$ and $n(e,e'\pi^-)X$, were simulated with the same generator used for the SoLID-SIDIS proposals, and their rates were calculated by matching the acceptance of scattered electrons and pions with the ones in DEMP. It is difficult to estimate how many percentage of the SIDIS target fragments contain protons, so we assumed the target fragments ("X") all contain one or more protons. This conservative assumption would cause the SIDIS rate being significantly overestimated.

However, considering other proton channels (like proton-knock-out during QE) and accidental events, it may still be a good estimation, although I would expect the SIDIS peak would be much broader.

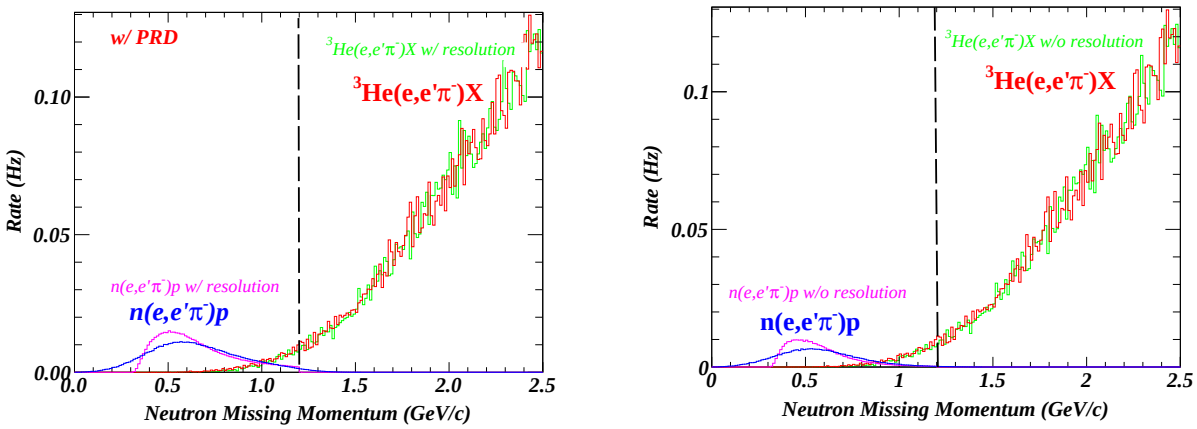

(a) w/ PRD

(b) w/o PRD

Figure 13: Missing momentum spectra of DEMP and SIDIS events. The missing momentum distributes are well separated between two processes and one can apply a cut at $P_{miss} < 1.2\ GeV/c$ (indicated by the black dash line) to remove most of SIDIS events.

Shown in Fig. 13, we reconstruct the missing momenta of both the DVMP and SIDIS processes and immediately discovered that the missing momentum distributions of two processes are well separated. The SIDIS background will be largely rejected when we apply a cut, $P_{miss} < 1.2\ GeV/c$.

We then reconstructed the missing mass spectra of the DEMP and SIDIS events w/ and w/o the missing momentum cuts, shown in Fig. 14. Befor applying the missing momentum cut, the SIDIS background overwhelms the DVMP peak (but note that the SIDIS rate is overestimated). When applying the cut, the DVMP peak dominates and the SIDIS background is largely suppressed. If we consider the fact that not every "X" in SIDIS contains a proton, the background should be negligible.

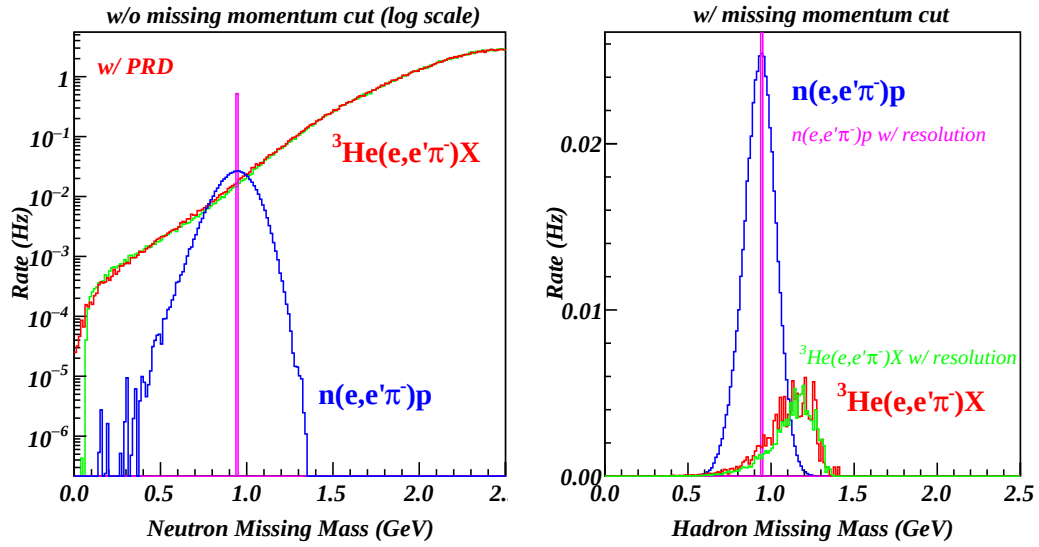

(a) w/ PRD

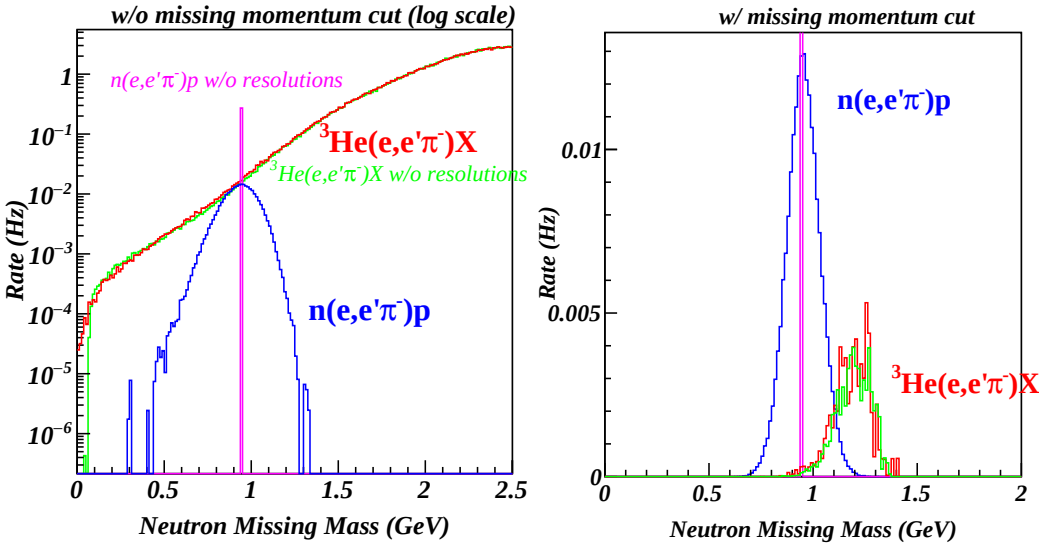

(b) w/o PRD

Figure 14: Missing mass spectra of DEMP and SIDIS events. Top (bottom) panel shows the missing mass distribution of DEMP events w/ (w/o) proton detection by a new PRD. The left (right) plot of each panel shows the background contamination from SIDIS events before (after) the missing momentum cut shown in Fig. 13. The SIDIS background is already small compared with DEMP events. The actual SIDIS background should be much smaller, since we overestimated the SIDIS rate by assuming all target fragments ("X") in the SIDIS process contain protons.

5 Systematic Uncertainties

The detector related systematic errors are expected to be similar to the ones given in the E12-10-006 proposal as well as in other SIDIS experiments with SoLID, as shown in Table 5.

Sources	Relative Value
Beam Polarization	2%
Target Polarization	3%
Acceptance	3%
Other Contamination	$< 5\%$
Radiation Correction	1%

Table 5: Expected systematic errors.

6 Summary

The transverse single-spin asymmetry in the exclusive $\vec{n}(e, e'\pi^-)p$ reaction has been noted as being especially sensitive to the spin-flip generalized parton distribution (GPD) $\tilde{E}$. Factorization studies have indicated that precocious scaling is likely to set in at moderate $Q^2 \sim 2 - 4$ GeV^2, as opposed to the absolute cross section, where scaling is not expected until $Q^2 > 10$ GeV^2. Furthermore, this observable has been noted as being important for the reliable extraction of the charged pion form factor from pion electroproduction.

This measurement is complementary to a proposal to measure the longitudinal photon, transverse nucleon, single-spin asymmetry $A_L^{\perp}$ with the SHMS+HMS in Hall C [**?**]. The good resolution and reproducible systematic uncertainties of the SHMS+HMS setup allow the L–T separation needed to reliably measure this quantity. However, a wide $-t$ coverage is needed to obtain a good understanding of the asymmetry, and it always been intended to complement the SHMS+HMS $A_L^{\perp}$ measurement with an unseparated $A_{UT}^{sin(\phi-\phi_s)}$ measurement using a large solid angle detector. The high luminosity capabilities of SoLID make it well-suited for this measurement. Since an L–T separation is not possible with SoLID, the observed asymmetry is expected to be diluted by the ratio of the longitudinal cross section to the unseparated cross section. This was also true for the pioneering HERMES measurements, which provided a valuable constraint to models for the $\tilde{E}$ GPD. Our measurement will also help to constrain longitudinal backgrounds possibly complicating the extraction of the pion form factor from electroproduction experiment data, with the aim of eventually extending the kinematic range over which reliable data can be acquired from electroproduction data.

A Monte Carlo Model of Deep Exclusive π^- Production From The Neutron

One of the primary goals of this proposed measurement is to extend our knowledge of the σ_L, σ_T, σ_{LT} and σ_{TT} to larger values of Q^2, $-t$ and W. Initial Monte Carlo studies require a model for experimentally unexplored region of kinematics. The electroproduction of charged pion is best described by the VR model [32]. A brief description of VR model is given in section 1.2. The scattering cross section for $n(ee'\pi^-)p$ in one-photon exchange is given by equation 12:

$$\frac{d^5\sigma}{dE'd\Omega_{e'}d\Omega_\pi} = \Gamma_V \frac{d^2\sigma}{d\Omega_\pi}. \tag{12}$$

The virtual photon flux factor Γ_V in Eq. 12 is defined as:

$$\Gamma_v = \frac{\alpha}{2\pi^2}\frac{E'}{E}\frac{K}{Q^2}\frac{1}{1-\epsilon}, \tag{13}$$

where α is the fine structure constant, K is the energy of real photon equal to the photon energy required to create a system with invariant mass equal to W and ϵ is the polarization of the virtual photon.

$$K = (W^2 - M_p^2)/(2M_p) \tag{14}$$

$$\epsilon = \left(1 + \frac{2|\mathbf{q}|^2}{Q^2}\tan^2\frac{\theta_e}{2}\right)^{-1}, \tag{15}$$

where θ_e is the scattering angle of scattered electron. The two-fold differential cross section $\frac{d^2\sigma}{d\Omega_\pi}$ in the lab frame can be expressed in terms of the invariant cross section in center of mass frame of photon and proton:

$$\frac{d^2\sigma}{d\Omega_\pi} = J\frac{d^2\sigma}{dtd\phi}, \tag{16}$$

where J is the Jacobian of transformation of coordinates from lab Ω_π to t and ϕ (CM). The invariant cross section of Eq. 16 can be expressed in four terms. Two terms correspond to the polarization states of the virtual photon (L and T) and two states correspond to the interference of polarization states (LT and TT),

$$2\pi\frac{d^2\sigma}{dtd\phi} = \epsilon\frac{d\sigma_{\rm L}}{dt} + \frac{d\sigma_{\rm T}}{dt} + \sqrt{2\epsilon(\epsilon+1)}\frac{d\sigma_{\rm LT}}{dt}\cos\phi + \epsilon\frac{d\sigma_{\rm TT}}{dt}\cos 2\phi \tag{17}$$

A.1 Data Constraints

Precise L/T separated experimental data of exclusive electroproduction of π^- on ^{2}H are available up to $Q^2 = 2.57$ GeV^2, $-t = 0.350$ GeV^2 and $W = 2.168$ GeV [33]. Precise L/T separated experimental data of exclusive electroproduction of π^+ on ^{1}H are available up to $Q^2 = 2.703$ GeV^2, $-t = 0.365$ GeV^2 and $W = 2.127$ GeV [34]. In Ref. [35] and Ref. [36], separated σ_L and σ_T are measured up to $Q^2 = 4.703$ GeV^2 and $W = 2.2$ GeV. CLAS experiment E99-105 measured the unseparated cross section at Q^2 up to 4.35 GeV^2 and $-t$ up to 4.5 GeV^2 [37]. The HERMES collaboration measured the unseparated cross section for $Q^2 = 3.44$ GeV^2 and 5.4 GeV^2 [38] at $W = 4$ GeV.

A.2 Model for Higher Q^2 Kinematics

The electroproduction of charged pion is best described by the VR model [32]. The VR model is a Regge model with a parameterization of deep inelastic scattering amplitude to improve the description of σ_T. The description of σ_L is constrained by a fit to our F_π data from Jlab [34]. In Fig. 15 we plotted the last six data points of table v of Ref. [33], our parameterization and VR model points for exactly same values of Q^2, $-t$ and W. It shows the comparison of the same points of $\sigma_{L,T,LT,TT}$ vs. Q^2.

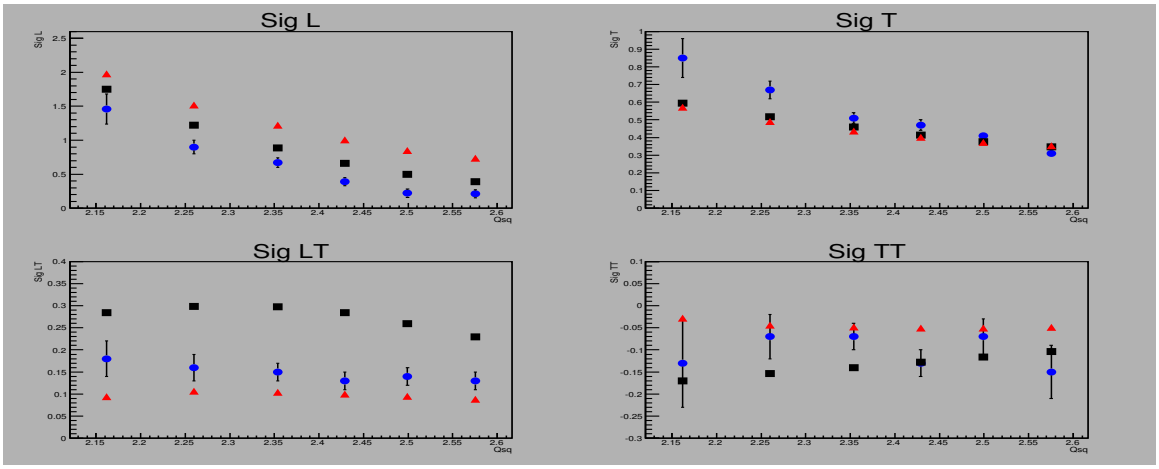

Figure 15: A comparison of last six points of table v of Ref. [33], VR model and our parameterization values vs. Q^2 of π^- electroproduction. Experimental data is shown in blue circles, VR model is shown in red triangles and our parameterization is shown in black boxes. In each graph value of $-t$ is decreasing left to right from maximum value 0.35 GeV^2 to 0.15 GeV^2. Value of W also decreases left to right from 2.2978 GeV to 2.1688 GeV.

A.3 Parameterization of σ_L, σ_T, σ_{LT}, & σ_{TT}

For exclusive DEMP in SoLID the kinematic region of interest for parameterization of $\sigma_{L,T,LT,TT}$ is Q^2 from 4.5 GeV to 7.5 GeV, $-t$ from 0 GeV^2 to 1.0 GeV^2 and we set $W = 3.0$ GeV. After the parameterization of $\sigma_{L,T,LT,TT}$ for $-t$ and Q^2, we used the same W dependence given by Ref. [34] which is $(W^2 - M^2)^{-2}$ where M is the proton mass. Our parameterization of all four cross sections is given in Eq. 18 to Eq. 21:

$$\sigma_L = \exp\left(P_1(Q^2) + |t| * P_1'(Q^2)\right) + \exp\left(P_2(Q^2) + |t| * P_2'(Q^2)\right) \tag{18}$$

$$\sigma_T = \frac{\exp\left(P_1(Q^2) + |t| * P_1'(Q^2)\right)}{P_1(|t|)} \tag{19}$$

$$\sigma_{LT} = P_5(t(Q^2)) \tag{20}$$

$$\sigma_{TT} = P_5(t(Q^2)), \tag{21}$$

where the parameters P_i are polynomial functions of ith order. Each coefficient (P_i) of fifth order equations Eq. 20 and Eq. 21 is a further second order polynomial of Q^2. Deep exclusive π^- events are

generated using a C++ code. The quality of parameterization is checked by plotting the parameterization functions of $\sigma_{L,T,LT,TT}$ versus the VR model as shown in Fig. 16.

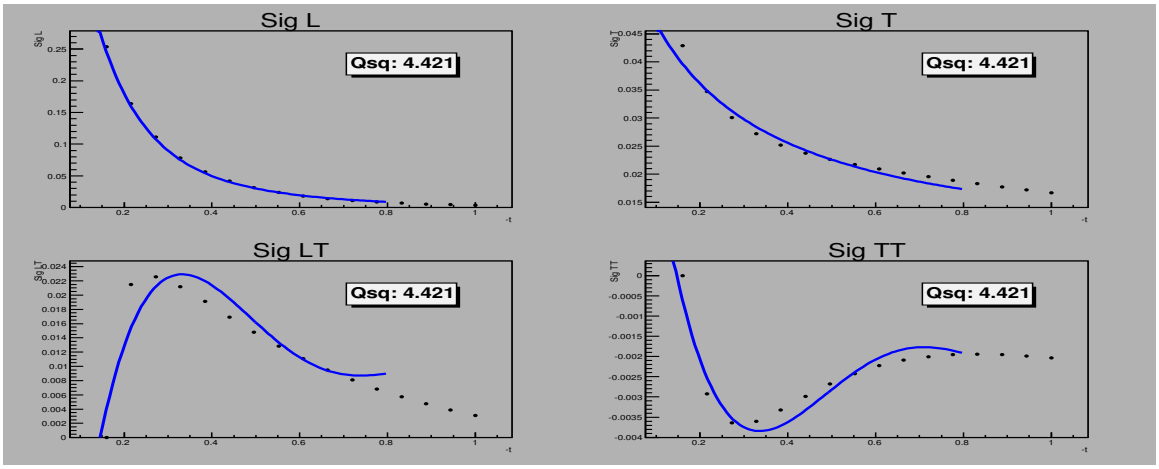

Figure 16: A comparison of parameterized $\sigma_{L,T,LT,TT}$ and VR model values at $Q^2 = 4.421$ GeV^2 and $W = 3.0$ GeV. Black points are VR model values and blue line is parameterized $\sigma_{L,T,LT,TT}$ given by equations Eq. 18 to Eq. 21.

Fig. 16 shows the comparison of parameterization of $\sigma_{L,T,LT,TT}$ and VR model points. The blue line is the parameterization curve and black points are the VR model points.

A.4 Single Spin Asymmetry (SSA) $\mathbf{A_L^{\perp}}$

It is shown in Ref. [39] that the generalized parton distribution ($\tilde{E}$) can be probed by measuring the single spin asymmetry(SSA). The SSA is defined in Eq. 22, where β is the angle between the transversely polarized target vector and the reaction plane, and $\sigma_L^{\pi^-}$ is the exclusive π^- cross section for longitudinal virtual photons. We parameterized the single spin asymmetry using the model of Ref. [39] at $x = 0.1$ and $x = 0.3$. Parameterization of SSA is shown in Fig. 17 and Eq. 23 is the parameterized function of single spin asymmetry.

$$\mathbf{A_L^{\perp}} = \frac{\int_0^{\pi} \mathbf{d}\beta \frac{\mathbf{d}\sigma_{\mathbf{L}}^{\pi^-}}{\mathbf{d}\beta} - \int_{\pi}^{\mathbf{2\pi}} \mathbf{d}\beta \frac{\mathbf{d}\sigma_{\mathbf{L}}^{\pi^-}}{\mathbf{d}\beta}}{\int_{\mathbf{0}}^{\mathbf{2\pi}} \mathbf{d}\beta \frac{\mathbf{d}\sigma_{\mathbf{L}}^{\pi^-}}{\mathbf{d}\beta}} \tag{22}$$

$$\mathbf{A_L^{\perp}} = \begin{cases} A_0 \left[1 - \exp^{[-\lambda \times (t - t_{min})]}\right] & \text{if } t \geq t_{min}, \\ 0 & \text{if } t < t_{min}. \end{cases} \tag{23}$$

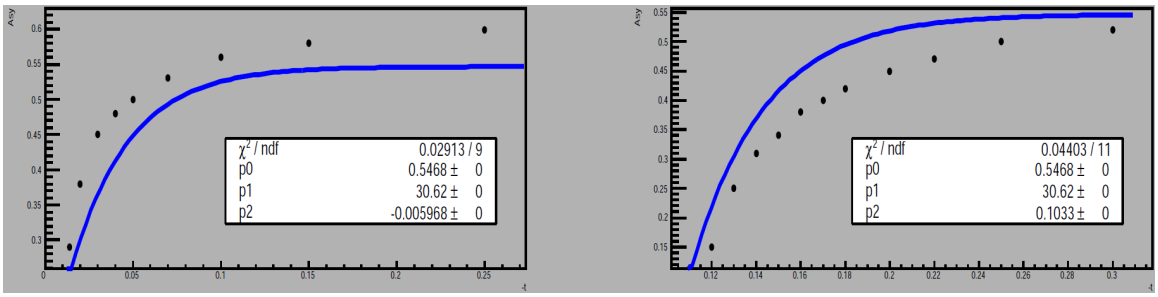

Figure 17: Parameterization of single spin asymmetry $\mathbf{A_L^{\perp}}$ vs. $-t$ at $Q^2 = 10$ GeV^2 in left graph $x = 0.1$ and in right graph $x = 0.3$ where the points are from the model defined in Ref. [39] and blue line is our parameterization function.

References

[1] A. Airapetian, Phys. Lett. **B 682** (2010) 345-350, arXiv:0907.2596 [hep-ex].

[2] PR12-12-005: D. Dutta, D. Gaskell, W. Hersman, G.M. Huber, et al., "The Longitudinal Photon, Transverse Nucleon, Single-Spin Asymmetry in Exclusive Pion Production".

[3] M. Diehl, Contribution to the eRHIC White Paper, arXiv:hep-ph/0010200.

[4] J.C. Collins, L. Frankfurt, M. Strikman, Phys. Rev. D **56** (1997) 2982.

[5] K. Goeke, M.V. Polyakov, M. Vanderhaeghen, Prog. Part. Nucl. Phys. **47** (2001) 401-515.

[6] A.V. Radyushkin, arXiv:hep-ph/0101225.

[7] A.W. Thomas, W. Weise, "The Structure of the Nucleon", J. Wiley-VCH, 2001.

[8] R.E. Marshak, Riazuddin, C.P. Ryan, "Theory of Weak Interactions in Particle Physics", J. Wiley, 1969.

[9] M. Penttinen, M.V. Polyakov, K. Goeke, Phys. Rev. C **62** (2000) 014024 1-11.

[10] A.V. Belitsky, D. Mueller, Phys. Lett. **B 513** (2001) 349-360.

[11] L.L. Frankfurt, P.V. Pobylitsa, M.V. Polyakov, M. Strikman, Phys. Rev. D **60** (1999) 014010 1-11.

[12] M. Vanderhaeghen, P.A.M. Guichon, M. Guidal, Phys. Rev. D **60** (1999) 094017 1-28.

[13] L.L. Frankfurt, M.V. Polyakov, M. Strikman, M. Vanderhaeghen, Phys. Rev. Lett. **84** (2000) 2589-2592.

[14] A.V. Belitsky, CIPANP 2003 proceedings. arXiv: hep-ph/0307256.

[15] L. Mankiewicz, G. Piller, A. Radyushkin, Eur. Phys. J. **C 10** (1999) 307-312.

[16] C.E. Carlson, J. Milana, Phys. Rev. Lett. **65** (1990) 1717.

[17] E12-06-101, "Measurement of the Charged Pion Form Factor to High Q^2", G.M. Huber, D. Gaskell, spokespersons.

[18] S. V. Goloskokov and P. Kroll, Eur. Phys. J. C **65**, 137 (2010), arXiv:0906.0460 [hep-ph].

[19] M. Diehl, S. Sapeta, Eur. Phys. J. C **41** (2005) 515, arXiv:hep-ph/0503023.

[20] S. V. Goloskokov and P. Kroll, private communications 2009-12.

[21] H.P. Blok, et al., Phys. Rev. C **78** (2008) 045202.

[22] pCDR for the Science and Experimental Equipment for the 12 GeV Upgrade of CEBAF, June, 2004. V. Burkert et al., PAC18 Review of the Science Driving the 12 GeV Upgrade, July, 2000.

[23] J. L. Friar et al., Phys. Rev. C 42, (1990) 2310; C. Ciofi degli Atti, and S. Scopetta, Phys. Lett. **B404**, (1997) 223; R.W. Schulze and P.U. Sauer, Phys. Rev. **C56** (1997) 2293; F. Bissey, A.W. Thomas, and I.R. Afnan, Phys. Rev. **C64**, (2001) 024004.

[24] Approved SoLID SIDIS experiment E12-10-006,
"Target Single Spin Asymmetry in Semi-Inclusive Deep-Inelastic $(e, e'\pi^{\pm}$' Reaction on a Transversely Polarized ^{3}He Target at 11 GeV",
$https://www.jlab.org/exp\_prog/proposals/14/E12-10-006A.pdf$

[25] SoLID Collaboration, "Solenoial Large Intensity Device Preliminary Conceptual Design Report," $http://hallaweb.jlab.org/12GeV/SoLID/files/solid\_precdr.pdf$

[26] Approved SoLID SIDIS experiment E12-11-007,
"Asymmetries in Semi-Inclusive Deep-Inelastic $(e, e'\pi^{\pm}$ Reactions on a Longitudinally Polarized ^{3}He Target at 8.8 and 11 GeV ",
$https://www.jlab.org/exp_prog/PACpage/PAC37/proposals/Proposals/New\%20Proposals/PR-11-007.pdf$

[27] Approved SoLID SIDIS experiment E12-11-108,
"Target Single Spin Asymmetry in Semi-Inclusive Deep-Inelastic $(e, e'\pi^{\pm}$ Reactions on a Transversely Polarized Proton Target",
$https://www.jlab.org/exp\_prog/proposals/11/PR12-11-108.pdf$

[28] Approved SoLID J/ψ experiment E12-12-006A,
"Near Threshold Electroproduction of J/ψ at 11 GeV",
$https://www.jlab.org/exp_prog/proposals/12/PR12-12-006.pdf$

[29] Approved SoLID SIDIS experiment E12-11-108A,
"Target Single Spin Asymmetry Measurements in the Inclusive Deep-Inelastic $vecN(e, e')$ Reaction on Transversely Polarized Proton and Neutron (^{3}He) Targets using the SoLID Spectrometer "
$https://www.jlab.org/exp_prog/proposals/14/E12-11-108A_E12-10-006A.pdf$

[30] Approved SoLID SIDIS experiment E12-10-006A,
"Dihadron Electroproduction in DIS with Transversely Polarized ^{3}He Target at 11 and 8.8 GeV",
$https://www.jlab.org/exp_prog/proposals/14/E12-10-006A.pdf$

[31] Approved SoLID PVDIS experiment E12-10-007,
"Precision Measurement of Parity-violation in Deep Inelastic Scattering Over a Broad Kinematic Range",
$https://www.jlab.org/exp\_prog/PACpage/PAC37/proposals/Proposals/Previously\%20Approved/E12-10-007.pdf$

[32] T. Vrancx and J. Ryckebusch., Phys. Rev. **C89**, 025203 (2014).

[33] G. M. Huber *et al.*, Phys. Rev. **C91**, 015202 (2015).

[34] H. Blok *et al.*, Phys. Rev. **C78**, 045202 (2008).

[35] T. Horn *et al.*, Phys. Rev. Lett **97**, 192001 (2006).

[36] T. Horn *et al.*, Phys. Rev. **C78**, 058201 (2008).

[37] http://clas.sinp.msu.ru/cgi-bin/jlab/db.cgi?eid=36;search=on

[38] A. Airapetian *et al.*, Phys. Lett. B. **659**, (2008).

[39] L. L. Frankfurt *et al.*, Phys. Rev. Lett. **84**, 2589 (2000).